

Ray-Optical Modeling of Wireless Coverage Enhancement using Engineered Electromagnetic Surfaces: Experimental Verification at 28 GHz

Y. de Jong^{#1}, R. Chaharmir^{#2}, S. Raut^{#3}, D. McLachlan[#], M. Zhang[#],
G. Bedrosian^{*4}, M. Schmiedekamp^{*}, J. DeLancey^{*}, R. Silber Belmonte^{*5}

[#]Communications Research Centre Canada, Ottawa, ON, Canada

^{*}Remcom, Inc., State College, PA, USA

{¹yvo.dejong, ²reza.chaharmir, ³shailesh.raut}@ised-isde.gc.ca, {⁴gary.bedrosian, ⁵ruth.belmonte}@remcom.com

Abstract—Results are presented of propagation experiments conducted to verify the accuracy of a novel ray-optical scattering model for engineered electromagnetic surfaces, a class of passive metasurfaces designed to enhance wireless signal coverage. The measurements were performed at 28 GHz, using a wideband channel sounder equipped with phased-array antennas. Measured results were compared to simulations performed with a commercial ray-tracing software tool incorporating the scattering model, showing excellent agreement for a 30°–60° diffuser deployed in a large office space.

Keywords—ray tracing, metasurfaces, millimeter wave measurements.

I. INTRODUCTION

Engineered electromagnetic surfaces (EESs) are a class of passive metasurfaces designed to artificially enhance wireless signal coverage [1]. They are fabricated by printing conductive or dielectric ink patterns on substrates such as plastic coatings, window glass, ceramic tile or drywall. These patterns consist of discrete, subwavelength unit cells whose scattering properties can be designed to control the spatial properties of the reflected and transmitted wavefronts. EESs often employ locally periodic unit-cell patterns, meaning that their scattering properties are modulated periodically over space, or at least approximately so over any sufficiently small subsurface. An example of a strictly periodic EES is the uniform grating, capable of deflecting incident waves in directions that do not obey Snell's law of reflection [2]. An example of a *locally* periodic EES is the reflective diffuser, which can be used to disperse incident signal power into a wider range of directions.

Ray tracing is the method of choice for simulating propagation characteristics in complex, electrically large environments such as office buildings and street canyons. Wireless InSite [3] is a commercial ray-tracing tool based on the uniform theory of diffraction (UTD). Its capabilities have recently been extended with a ray-optical EES scattering model based on theory presented in [4]. This model is applicable to locally periodic metasurfaces of polygonal shape and describes their scattered fields in terms of reflected, transmitted and diffracted rays interacting at so-called *critical* surface points. Unlike for conventional materials, these rays do not generally adhere to geometrical constraints like Snell's law and the Keller cone.

This paper describes Wireless InSite's implementation of the scattering model, and presents measured and simulated propagation data for a large indoor office environment. These results demonstrate the feasibility of wireless coverage enhancement by strategically deploying EESs, and of predicting their effects with the aid of ray-tracing software.

II. EES SCATTERING MODEL

The ray-optical EES scattering model introduced in [4] provides a uniform ray description of electromagnetic wave scattering by locally periodic metasurfaces. It describes the homogenized properties of such metasurfaces in terms of periodic functions of a location-dependent parameter ψ [4, Eq. (12)]. This parameter is referred to as the *phase* of the surface profile, expressed in units of length; by definition, the period of the surface profile with respect to ψ is equal to the wavelength, λ . The phase is assumed to be a continuous and smooth function of the rectangular surface coordinates u_1 and u_2 . Users of the model define the overall shape of the surface profile by specifying the phase *gradient* [4, Eq. (13)], a unitless, two-dimensional vector, at the points of a rectangular surface grid. The grid spacing can be much larger than the wavelength, but must be small enough to enable accurate interpolation. Without any loss of generality, ψ is assumed to be zero at the origin of the (u_1, u_2) coordinate system.

The precise variation of surface properties along a period of the profile is defined by the spatial Fourier coefficients

$$F^{(m)} = \frac{1}{\lambda} \int_0^\lambda F(\psi) e^{-jk_m\psi} d\psi, \quad (1)$$

where F is a placeholder for the quantities (specified in the next paragraph) used to characterize the localized properties; m is the so-called spatial mode number, and $k = 2\pi/\lambda$ is the free-space wavenumber. In practice, these coefficients become negligibly small for large $|m|$ and are specified only up to a fixed mode truncation number M , i.e., $|m| \leq M$.

Wireless InSite describes the scattering properties of EES materials in terms of the isotropic electric and magnetic sheet impedances [5], defined by the user via an EES material specification file [3]. The impedance variation is assumed to be identical for every period of the surface profile and is therefore

defined by two sets of $2M + 1$ spatial Fourier coefficients, also referred to as the electric and magnetic mode impedances. The EES material file also defines the surface grid and contains a table of the phase gradient for each grid point.

Rays incident on a locally periodic metasurface give rise to discrete spectra of reflected, transmitted and/or diffracted rays, each with a different scattering direction associated with the mode number m . Of these rays, only those with $m = 0$ adhere to Snell's reflection and transmission laws and the Keller cone [4]. In order to limit computational complexity, the Wireless InSite prediction engine traces the scattered rays for only one mode number per EES object. This mode number must be specified in the EES material file; the default value is $m = 1$. Wireless InSite also requires that, for any sequence of objects encountered by a ray propagating between two points in a scene, the EES objects support only one specular point per geometry face and one diffraction point per geometry edge. This condition is satisfied if none of the EES objects have a concave-upward phase distribution, capable of focusing an incident field.

III. PROPAGATION MEASUREMENTS

A. Equipment

The verification measurements were performed using a mobile millimeter-wave channel sounding system designed to characterize the impulse response and directional channel properties at 28 GHz in non-stationary environments, including scenarios where the transmitter (Tx) and/or receiver (Rx) terminals are in motion. Both terminals consist of a sensor platform, a radio frequency (RF) signal generation or acquisition subsystem, and a control subsystem. The Tx sensor platform consists of a 64-element (8×8), electronically steerable phased-array antenna (PAA), and also includes a panoramic video camera and a Lidar device. The Rx sensor platform is identical except that it uses four PAA units offset by 90° in azimuth to provide omnidirectional coverage. These platforms were mounted on top of rolling equipment racks, such that the PAA apertures were 1.25 m above the floor.

The system was programmed to continually measure the channel response by transmitting and receiving a chirp sounding waveform [6], while simultaneously steering the PAA beam directions according to a user-specified, double-directional scan sequence. The set of channel data and associated metadata measured during one cycle of the scan pattern is referred to as a snapshot; the snapshot rate was 2 Hz. The sounding waveform had a bandwidth of 1 GHz, a pulse duration of $5 \mu\text{s}$, and a pulse repetition interval of $100 \mu\text{s}$. The Tx beam direction was fixed and the Rx beams were steered from -40° to 40° in azimuth and elevation with respect to their boresights, in steps of 10° . The same beam pattern type was selected for all PAA units; its boresight half-power beamwidth is 18° , and its highest sidelobe level is approximately -20 dB.

B. Environment

The measurements were conducted in a large collaborative office space, shown in Fig. 1. This space features a curved

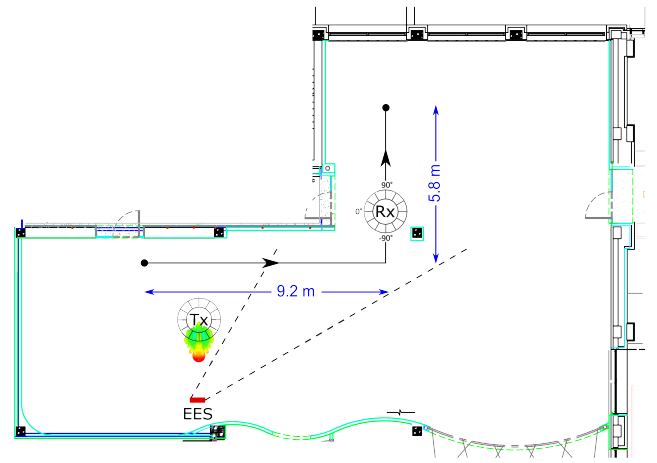


Fig. 1. Plan view of the office environment showing the locations of the Tx, the EES pedestal, and the Rx route. The dashed lines indicate the range of deflection angles of the 30° - 60° diffuser (for normal incidence).

projection screen (lower right) next to a curved interior wall containing an open doorway. Apart from one exterior wall (top right), the walls are made of steel-framed drywall and filled with fiberglass insulation. The three entrance doors are made of glass and have metal frames. The concrete floor is covered with linoleum tiles. The floor slab above is supported by concrete columns and the ceiling space directly underneath is mostly open, with exposed ductwork and suspended track lighting. People and furniture (not shown in Fig. 1) were also present in the room; care was taken to keep them away from the area where the measurements were taken.

The Tx was parked at a fixed location and oriented such that its beam was pointed at a (curved) wall, thereby intentionally creating challenging coverage conditions in large parts of the room. A wooden pedestal capable of holding various types of EESs was placed in front of this wall, and served to emulate the deployment of a wall-mounted EES. The measurements reported here were conducted for a square, 30° - 60° diffuser, designed to azimuthally spread normally incident power over the range of deflection angles indicated by the dashed lines in Fig. 1. The center of the EES was at 1.25 m above floor level, the same height as the Tx and Rx PAA units; its width and height were 0.56 m. For comparison, a reference measurement was conducted with no EES present. The Rx was moved along a measurement route consisting of two straight subroutes connected by a 90° left turn, at an approximately constant speed of 0.2 m/s. Its orientation with respect to the room was kept the same on both subroutes.

C. Results

The measured data were converted to calibrated power delay profiles by correlating the received signal waveforms with a replica of the sounding waveform, while correcting for the Tx power, antenna gain patterns, and various hardware and processing gains and losses. The power delay profiles for each snapshot were then integrated over delay and overlaid on the corresponding panoramic still image to produce directional heatmaps like those in Fig. 2, which visualize the directional

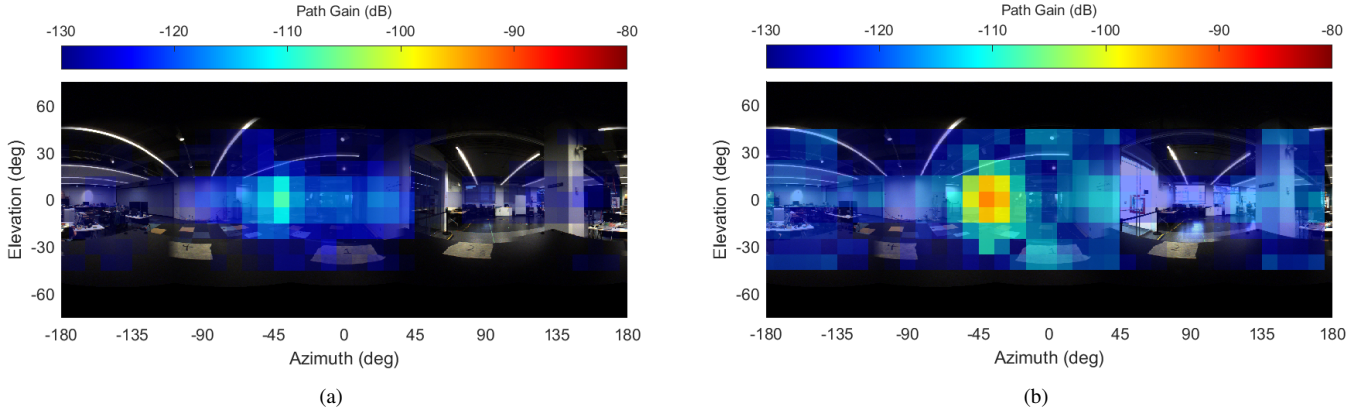


Fig. 2. Azimuth-elevation multipath gain profiles measured at 9.2 m from the beginning of the Rx route shown in Fig. 1: (a) without an EES present; (b) for the 30° – 60° diffuser. The dominant multipath contribution in (b) is due to a reflection from the EES; that in (a) is due to a wall reflection.

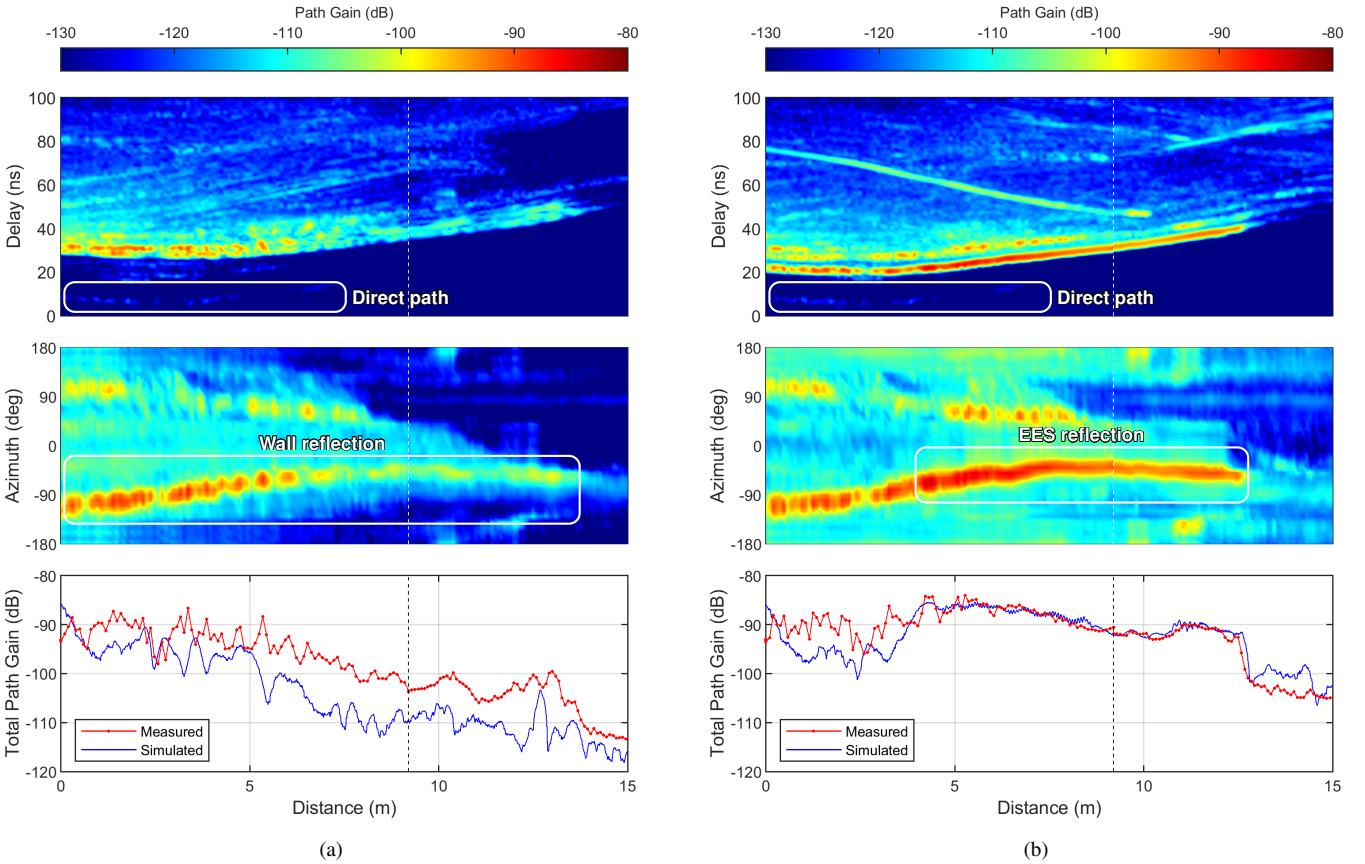


Fig. 3. Measured multipath gain distributions versus distance along the Rx route shown in Fig. 1: (a) without an EES present; (b) for the 30° – 60° diffuser. Vertical dashed lines indicate the 90° left turn at a distance of 9.2 m. The bottom-most plots show total path gain and include simulated (ray tracing) results.

distribution of multipath gain from the perspective of the Rx. The main peak in Fig. 2(a) is consistent with a reflection from the curved wall behind the EES pedestal, most likely via a (highly reflective) wall stud. Fig. 2(b) shows that the EES increases the signal level at the selected location by creating a new propagation path with higher gain (approximately 10 dB).

Fig. 3 provides additional detail about the multipath composition of the received signal and its evolution along the measurement route; it also shows the total path gain, obtained by integrating over direction-of-arrival as well as

delay. In both subfigures of Fig. 3, the direct propagation path is weak compared to several longer paths that interact with the environment; this is due to the directionality and orientation of the Tx antenna beam, which was pointed away from the Rx route (see Fig. 1). With no EES present, the main received signal contribution reflects from the curved wall behind the EES pedestal. The intermittent nature of the reflected path is believed to be due to the wall studs. The main observation from Fig. 3 is that the diffuser creates a new, high-gain propagation path that enhances signal coverage along most of the route.

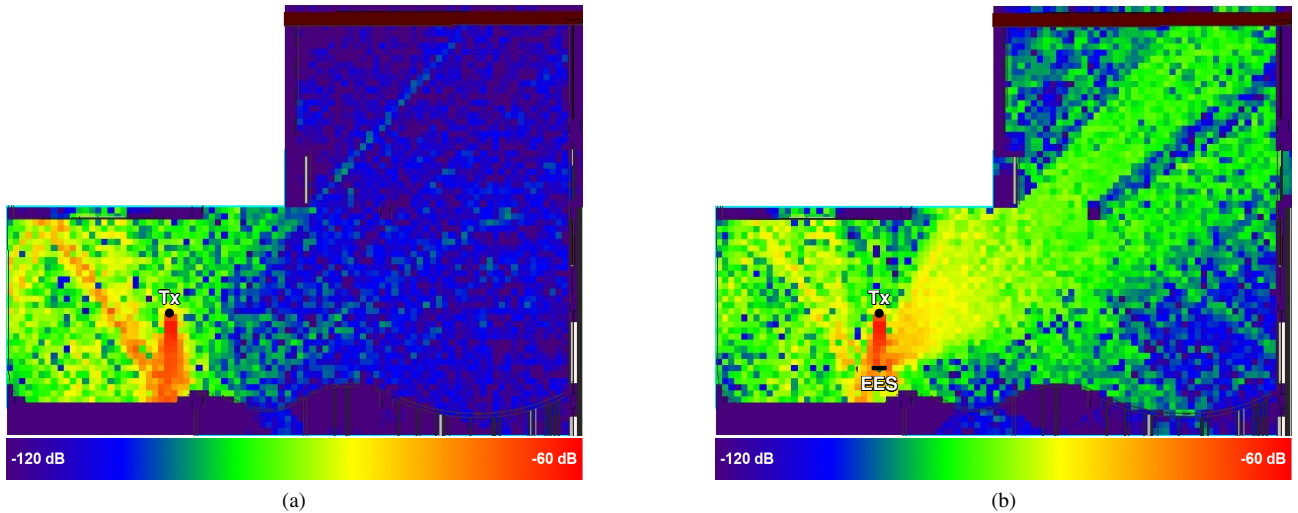


Fig. 4. Simulated point-to-area path gain for the setup shown in Fig. 1: (a) without an EES present; (b) for the 30°–60° diffuser.

IV. COMPARISON TO RAY-TRACING SIMULATIONS

Wireless InSite and a 3D model of the office environment in Fig. 1 were used to simulate narrowband path gain for the two scenarios (with and without a 30°–60° diffuser) described in Section III. The maximum numbers of reflections, transmissions and diffractions per ray were set to 4, 2 and 1, respectively, and the EES mode truncation number was set to $M = 8$. The 3D scene model contained detailed descriptions of the geometrical and dielectric material properties of room elements such as the doors, windows and curved wall, but did not include furniture or people. The internal composition of the walls, including the metal framing studs, was approximated by a two-layer dielectric material consisting of 1.3 cm of drywall with a metal backing. The simulated Tx antenna was assigned the (fixed) PAA beam pattern used for the measurements, and the Rx antenna was modeled as being isotropic.

Results of the ray-tracing simulations are shown in Fig. 4 and in the bottom-most plots of Fig. 3, where they are compared to the measured path gain data. To smooth out rapid fluctuations due to multipath interference, the simulated path gain data in Fig. 3 were spatially averaged using a moving-average window of length 20λ . Like the measurements, the simulations indicate that the presence of the diffuser results in marked signal coverage improvement in large parts of the room. The simulated results in Fig. 3(b) show excellent agreement with the measured path gain along the middle section of the route, where the total path gain is dominated by the diffuser. The simulations are seen to underestimate the path gain due to the office environment itself, i.e., for most of the measurement route in Fig. 3(a) and for the first section in Fig. 3(b). This discrepancy is believed to be caused by our approximate wall model, and is currently being investigated in more detail.

V. CONCLUSIONS

This paper has presented results of wideband and directional propagation measurements conducted to verify the accuracy of a novel ray-optical EES scattering model. These results show excellent agreement between measured and simulated properties (amplitude, delay and direction-of-arrival) of the “artificial” propagation path created by the EES. The comparison has also highlighted the importance of correctly modeling other relevant details of the environment – in our specific case, the material composition of interior walls. The new simulation capability demonstrated in this paper will enable wireless engineers to analyze the effects of EES deployments in large, real-world propagation environments.

ACKNOWLEDGMENTS

The authors would like to thank T. Smith, M. Basar and D. Liu for their assistance with the measurements, and H. Zhu and S. Perras for managing the collaboration between CRC and Remcom.

REFERENCES

- [1] A. Petosa, N. Gagnon, C. Amaya, M. Li, S. Raut, J. Ethier and R. Chaharmir, “Characterization and enhancement of the environment for 5G millimetre-wave broadband mobile communications”, presented at *12th European Conf. on Antennas Propagat. (EuCAP 2018)*, London, UK, Apr. 2018.
- [2] C. A. Balanis, *Advanced Engineering Electromagnetics*, Wiley, New York, NY, 1989.
- [3] Remcom Inc., *Wireless InSite: 3D Wireless Communication and Propagation Prediction Software*, Reference Manual, Version 3.4.4, Dec. 2022.
- [4] Y. L. C. de Jong, “Uniform ray description of physical optics scattering by finite locally periodic metasurfaces”, *IEEE Trans. Antennas Propagat.*, vol. 70, no. 4, pp. 2949–2959, Apr. 2022.
- [5] X. Liu, F. Yang, M. Li, and S. Xu, “Generalized boundary conditions in surface electromagnetics: fundamental theorems and surface characterizations”, *Appl. Sci.*, no. 9, 2019.
- [6] S. Salous, *Radio propagation measurement and channel modelling*, Chichester, UK: Wiley, 2013.